Catalysis Science & Technology

ROYAL SOCIETY OF CHEMISTRY

PAPER

View Article Online
View Journal | View Issue

Cite this: *Catal. Sci. Technol.*, 2021, 11, 4051

Carbothermally generated copper–molybdenum carbide supported on graphite for the CO_2 hydrogenation to methanol†

A. B. Dongil, *[a] J. M. Conesa, [b] L. Pastor-Pérez, [c] A. Sepúlveda-Escribano, [d] A. Guerrero-Ruiz [be] and I. Rodríguez-Ramos [ae]

The carbothermal synthesis of monometallic and bimetallic molybdenum carbide and copper, supported on high surface area graphite (H), has been studied by *in situ* XRD, XPS, D_2-TPD, TEM/STEM, TG-mass spectrometry, and N_2 adsorption. The catalysts were prepared using H_2 at 600 °C or 700 °C and tested in the hydrogenation of CO_2 to methanol. Molybdenum carbide and oxycarbide phases were obtained, as well as hydride species, at 600 °C on both monometallic Mo_xC/H and bimetallic $CuMo_xC$/H in a similar proportion. Upon increasing the temperature up to 700 °C, the formation of metallic Mo is favourable. Although this is observed on supported Mo_xC and $CuMo_xC$, the bimetallic sample is less affected by the formation of the hydride, and molybdenum carbide is also observed upon treatment at 700 °C. With regards to the catalytic performance, supported monometallic copper was not active, but copper increased the activity and selectivity of the molybdenum carbide. The yield of methanol per catalyst's weight increases upon increasing the copper loading, indicating that a cooperation reaction takes place between the smallest Cu particles in contact with the molybdenum phase. The catalysts synthesized at 700 °C are less active and less selective to methanol favouring the reverse water gas shift under the studied conditions. Interestingly, the catalysts are stable under the reaction conditions, and the detected phases by XRD of the spent catalysts suggest that the hydride species favoured transformations involving $MoO_xC_yH_z \leftrightarrow \beta$-$Mo_2C$.

Received 8th March 2021,
Accepted 29th March 2021

DOI: 10.1039/d1cy00410g

rsc.li/catalysis

1. Introduction

The need for diminishing carbon dioxide emissions to comply with the target of not surpassing 2 °C increase in the Earth temperature during this century has prompted several strategies to achieve such an objective while maintaining our current industrial model. The transformation into other energy models is specially challenging for many industries such as petrochemical, steel or cement which are among the largest CO_2 emitters. Besides the direct use of CO_2, attention has been paid to its transformation into other chemicals so that it can be considered as a valuable chemical platform. This would be an interesting alternative for industries that cannot avoid CO_2 emissions in their production and they can use the CO_2 by-product as a raw material in their own facilities. In this sense, the hydrogenation of CO_2 to CH_4 or CH_3OH presents an optimal solution. Several heterogeneous catalysts have been studied, and many of them are based on the traditional system used for CO hydrogenation, Cu/ZnO, and others based on noble metals.[1,2]

During the last few years, transition metal carbides have been attracting great attention as excellent hydrogenation catalysts, with catalytic performances that can reach or even surpass those of noble metals, with the advantage of their larger availability.[3] For the transformation of CO_2 into methanol, molybdenum carbide has been successfully employed in the liquid phase, the bimetallic copper–molybdenum carbide being more selective to methanol than metallic iron and cobalt, and just slightly less selective than palladium.[4] Other bimetallic systems formed with molybdenum carbide together with Au or Co have been compared to Cu–molybdenum carbide and it has been found that Cu promotes the methanol synthesis.[5,6]

[a] *Instituto de Catálisis y Petroleoquímica, CSIC, c/Marie Curie No. 2, Cantoblanco, 28049 Madrid, Spain. E-mail: a.dongil@csic.es*
[b] *Dpto. Química Inorgánica y Técnica, Facultad de Ciencias UNED, Senda del Rey 9, 28040 Madrid, Spain*
[c] *Department of Chemical and Process Engineering, University of Surrey, Guildford, GU2 7XH, UK*
[d] *Laboratorio de Materiales Avanzados, Departamento de Química Inorgánica – Instituto Universitario de Materiales de Alicante, Universidad de Alicante, Apartado 99, E-03080 Alicante, Spain*
[e] *UA UNED-ICP(CSIC), Grupo de Diseño y Aplicación de Catalizadores Heterogéneos, Madrid, Spain*

† Electronic supplementary information (ESI) available. See DOI: 10.1039/d1cy00410g

Several methods have been reported to synthesise molybdenum carbide using hydrocarbon/hydrogen mixtures at temperatures of up to 700–800 °C. However, the resulting catalysts are usually covered by graphitic carbon, and the surface areas are low, *i.e.* around 30 m^2 g^{-1}, for catalytic applications.[7] To overcome these limitations, other alternative synthetic procedures have been reported in which organic precursors are employed, but still the coverage of the active phase with polymeric carbon appears to occur.[8–10]

In order to find a suitable solution, carbon supports have been employed and a hydrogen atmosphere was used directly to obtain the corresponding carbide, using the support as a carbon source. This method, known as carbothermal reduction, has been employed with supports having different structures such as activated carbon, carbon nanofibers or carbon nanotubes, and different results regarding the molybdenum carbide phase have been reported.[11–13] These catalysts have been tested for several relevant industrial reactions such as methanol steam reforming, hydrodeoxygenation of stearic acid and also CO_2 hydrogenation, and correlation between the active phase and the catalytic results has been attempted.

Nonetheless, the identification of the carbide phase and quantitative determination of the stoichiometry is a challenging task in these carbon-based systems, and different results are reported in the literature. However, carbon is a very attractive support since it can provide carbon atoms for carburization, eliminating the need for an additional carbon source. The precise structure of the support also influences the structure of the resulting carbide.[11–13]

Despite the research performed so far, less literature is found related to supported molybdenum carbide catalysts applied on this reaction. Hence, we have studied the synthesis of copper–molybdenum carbide catalysts on a commercial graphitic support with a high surface area and evaluated the effect of copper and carburization temperature on the physicochemical and catalytic performance of these catalytic materials.

2. Results and discussion

2.1 Active phase characterization

In situ XRD in the range of 2θ = 33–60° is shown in Fig. 1 and the whole pattern is shown in Fig. S1.† The XRD patterns of Mo_xC/H and $CuMo_xC$/H treated at 600 °C under H_2 display diffraction peaks with maxima at 2θ of 36.9–37.1° and 53.6°, and the wideness of both peaks suggests that they might include more than one contribution. According to reference patterns, the first peak may contain contributions from either MoO_xC_y and/or MoO_2, and the second peak from MoO_2.[14] However, the possibility of these peaks including diffractions of hydride species cannot be disregarded as will be later explained. As expected, $CuMo_xC$/H also displays diffractions at around 43.1° and 50.0°, which are assigned to the (111) and (200) planes of metallic copper (JCPDS 04-0836). However, the peak at 2θ of 50.0° shifted to lower angles,

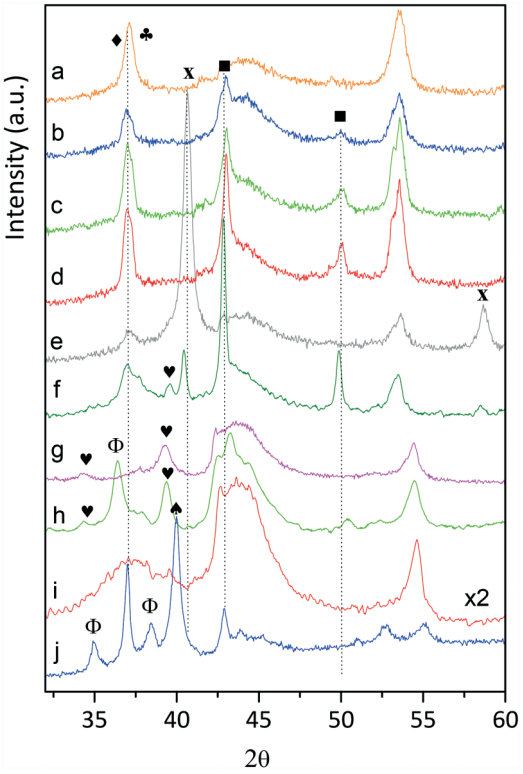

Fig. 1 *In situ* XRD patterns of the catalysts under H_2. a) Mo_xC/H; b) $1CuMo_xC$/H; c) $3CuMo_xC$/H; d) $CuMo_xC$/H; e) Mo_xC/H-700; f) $CuMo_xC$/H700. XRD patterns of the spent catalyst after the reaction at 230 °C: g) Mo_xC/H-PR; h) $CuMo_xC$/H-PR; i) Mo_xC/H700-PR; j) $CuMo_xC$/H-700-PR. ♥ β-Mo_2C; ♦ MoO_xC_y; ♣ MoO_2/$MoO_xC_yH_z$; ♠ MoO_3; X Mo^0; ΦCuO ■ Cu(0).

which could be due to the additional contribution of MoO_3 whose (002) plane appears at 49.1° (JCPDS-PDF 76-1003). The absence of additional diffractions corresponding to Cu_xC that would appear at around 2θ of 36.0° indicates that under the employed conditions its formation is not favourable.[15] This was also verified by XPS analyses, which showed no contributions attributed to Cu_xC, as shown in Fig. S2.†

Interestingly, upon heating at 700 °C, the most intense diffraction peaks of Mo_xC/H appeared at 40.6° and 58.7° which correspond to the (110) and (200) planes of the cubic structure of Mo^0 (JCPDS 42-1120), respectively. Under these conditions, the peak at 2θ of 37.1° is still observed, but its intensity is clearly lower than that of the sample carburized at 600 °C. Similarly, the catalyst $CuMo_xC$/H prepared at 700 °C led to a pattern different to that observed at 600 °C, since the diffraction peaks at 2θ of 36.9°, 37.7° and 39.5° are now present. In this case, it appears that the sample contains contributions attributed to MoO_xC_y, the first peak, and attributed to the (002) and (101) planes of the β-Mo_2C hcp phase, the last two peaks (JCPDS-PDF 77-0720). As observed for the Cu-free catalyst treated at 700 °C, diffractions at 2θ of 40.6° and 58.7° assigned to Mo^0 appear but their relative intensity compared to those assigned to MoO_xC_y and β-Mo_2C are lower.

The nature of the molybdenum phases was further studied by XPS of the carburized samples using the Mo 3d region, as

Table 1 XPS Mo 3d region binding energies: species and percentage (%) in brackets

	MoO_x	MoO_xC_y	Mo_xC	Mo^0
Catalyst	$Mo^{5+/6+}$	$Mo^{\delta+}$	Mo^{2+}	Mo^0
Mo_xC/H	231.6 (5)	229.4 (38)	228.5 (57)	—
$CuMo_xC$/H	231.1 (10)	229.4 (39)	228.6 (51)	—
Mo_xC/H700	232.1 (23)	229.6 (10)	228.5 (22)	227.7 (45)
$CuMo_xC$/H700	232.1 (19)	229.6 (13)	228.5 (22)	227.9 (44)

shown in Fig. S2,† from which the atomic contributions were obtained and are shown in Table 1. The Mo $3d_{3/5}$ region displayed several contributions which can be assigned to the following oxidation states: Mo^0 (227.7–227.9 eV), Mo^{2+} (228.5–228.6 eV), $Mo^{\delta+}$ (229.4–229.6 eV), Mo^{5+} (231.2–231.6 eV) and Mo^{6+} (232.1 eV). Mo^{2+} corresponds to Mo in Mo–C bonds, while Mo^{5+} and Mo^{6+} are the species of MoO_3 and Mo_2O_5, respectively.[16] Although MoO_3 appears due to incomplete carburization, the contribution of Mo_2O_5 is likely due to the reduction of the Mo^{6+} species under the high vacuum of the XPS analysis chamber. In addition, $Mo^{\delta+}$ is an intermediate oxidation state between +4 and +2 that has been ascribed to MoO_xC_y species, which agrees with the phases identified by XRD.[17,18]

The XPS spectra indicated that a similar MoO_xC_y/Mo_xC ratio is found on Mo_xC/H and $CuMo_xC$ and that, in fact, the concentration of molybdenum carbide is more significant than what the XRD patterns showed. This is not surprising as the TEM images in Fig. 2 and S3† proved that a large fraction of molybdenum carbide is highly dispersed. Also, the XPS results confirm the presence of Mo^0 on the samples carburized at 700 °C. Moreover, a similar relative proportion of Mo species estimated by XPS on the catalysts prepared at 700 °C agrees quite well with the comparable decrease of methanol yield obtained with these catalysts compared to their counterparts synthesized at 600 °C, which is in the range of 22–25% (Fig. 7).

In order to obtain more insight into the catalytic system, D_2-TPD experiments of the carburised samples were performed. Before the experiments, the catalysts were subjected to D_2 pulses at room temperature. The profiles of desorbed gases from Cu/H and the support alone, as shown in Fig. S4,† did not show any desorption in the whole temperature range. However, the profiles of the samples Mo_x-C and $CuMo_xC$ exhibited the evolution of m/z = 2 at temperatures of *ca.* 500 °C. This result suggested that during catalyst activation, metal hydride nanoparticles are formed. The hydride formation was further verified by performing the D_2-TPD experiment on a sample previously reduced under D_2, as shown in Fig. 3. The reduction with deuterium followed by the desorption experiment proved the presence of the hydride since m/z = 3 ascribed to HD is also observed as a result of the hydrogen atom exchange.

These experiments showed that a hydride is formed on Mo_xC or $CuMo_xC$ at temperatures above 400 °C and that neither Mo_xC nor $CuMo_xC$ chemisorbed H_2 at room temperature. The presence of hydride species cannot be accurately detected by XRD or XPS since perturbations due to H atoms are negligible, and their contribution would be included in the observed species.

The synthesis of molybdenum carbides by the carbothermal method using H_2 and carbon supports takes place through several steps that we have previously identified by XANES.[14] After the decomposition of the molybdate precursor into MoO_3, oxycarbide starts to be formed at *ca.* 300 °C, which is then converted into β-Mo_2C thanks to the contribution of carbon atoms from the support (reaction (1)). When the synthesis is carried out using hydrogen, it may help in the reduction process thanks to its diffusion coefficient. The higher Mo/C ratio, as shown in Table 2, for the samples treated at 700 °C agrees with the breakage of the crystallites during the synthesis, reported recently for Re carbides also supported on carbon.[19] Such small nanoparticles cannot be accurately detected by TEM and the average particle size distribution, as shown in Table 1, is quite similar for the catalyst.

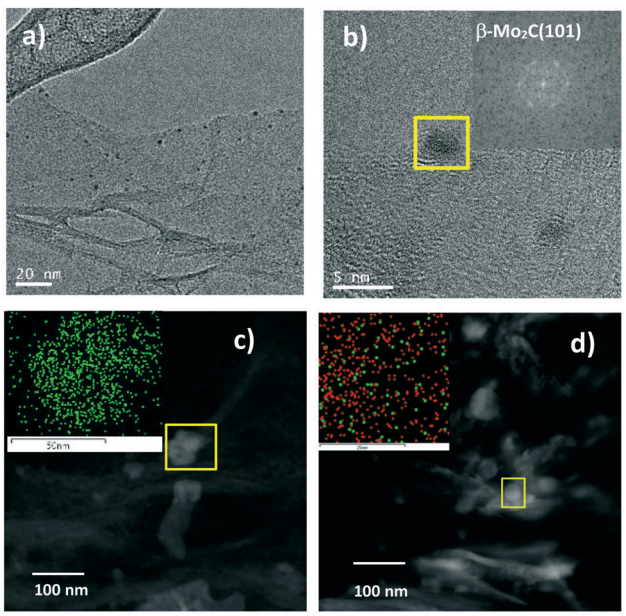

Fig. 2 Representative TEM/HRTEM images of $CuMo_xC$/H a) and b) higher magnification and the corresponding fast-Fourier transform (FFT) pattern; c) and d) STEM images of $CuMo_xC$/H with the mapping of Cu (green) and Mo (red).

Table 2 Textural and physical–chemical properties of the catalysts and XPS metal ratios

	Mo dp	S_{BET}	XPS ratio	
Catalyst	TEM (nm)	($m^2\ g^{-1}$)	Mo/C	Cu/C
Cu/H	—	307	—	
Mo_xC/H	1.8 ± 0.2	328	0.007	—
$CuMo_xC$/H	2.1 ± 0.3	205	0.013	0.231
Mo_xC/H-700	1.9 ± 0.3	304	0.015	—
$CuMo_xC$/H-700	2.0 ± 0.3	202	0.036	0.327

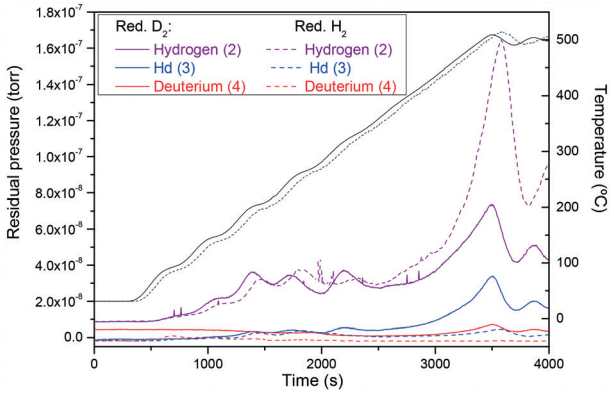

Fig. 3 MS profiles after D_2 adsorption on $CuMo_xC$ reduced under D_2 (solid) and H_2 (dashed).

$$MoO_3 + C^* + H_2 \rightarrow MoO_xC_y + H_2O \rightarrow \beta\text{-}Mo_2C + CO \quad (1)$$

One possibility to explain the reduction to Mo^0 could be that not enough reactive carbon, C* as shown in reaction (1), is available on the support, *e.g.* CH_4, to carry out the carburization of the molybdenum oxides and oxycarbides. In this context, the formation of Mo^0 could be favourable in a mechanism involving the previously formed hydride.

The carburization process under H_2 was also studied using mass spectrometry to follow the evolved masses and the results of m/z = 18, 17 and 15 are shown in Fig. 4. It can be observed that the profiles for the Mo_xC/H and $CuMo_xC/H$ samples are quite different.

On the one hand, for the sample Mo_xC/H, the ratios of m/z = 18 and 17 indicate that they are due to water and ammonia desorption, representative of chemical surface changes such as precursor decomposition and Mo oxide reduction. The absence of m/z = 15 in the whole range of temperatures, which should correspond to CH_4 evolution, is not conclusive regarding the formation of oxycarbide and carbide species which are certainly identified by XPS. The evolution of CO, m/z = 28, from the support, as shown in Fig. S5,† could also be responsible for metal carburization although the intensity is also low. Nevertheless, the intense peak of m/z = 18 due to H_2O at temperatures above 600 °C, along with the XRD and XPS results, suggests that the previously formed molybdenum species were transformed into Mo^0 in that temperature range. Reactions of the type $MoO_xH_z \rightarrow Mo^0 + H_2O$ can be suggested. So, in agreement with XRD, the reduction to Mo^0 is favourable on these samples above 600 °C.

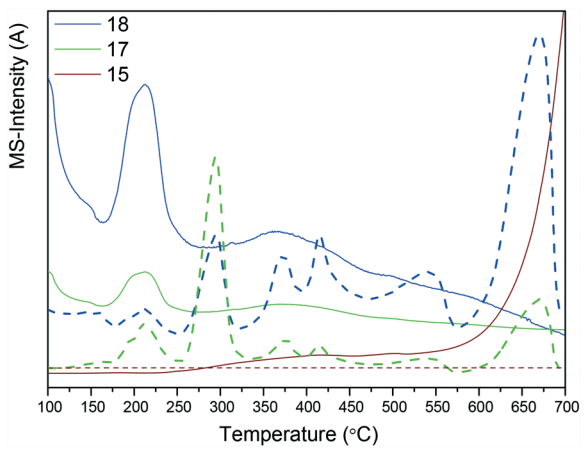

Fig. 4 MS profiles during H_2-TPR of the impregnated samples. Mo_xC/H (dashed) and $CuMo_xC/H$ (solid).

On the other hand, for the sample $CuMo_xC/H$, the ratios of m/z = 18 and 17 can be ascribed mainly to water desorption at temperatures below 500 °C. The most interesting feature of the mass profile of the $CuMo_xC/H$ sample compared to Mo_xC/H is the appearance of m/z = 15 in a proportion that can be undoubtedly ascribed to CH_4 evolution. This mass is already envisaged in the range of 300–500 °C, with maxima at around 400 and 450 °C, and then at 600 °C for $CuMo_xC/H$, an intense m/z = 15 signal is observed. This suggests that different proportions of intermediates and/or different paths are followed for Mo_xC/H and $CuMo_xC/H$, and that copper possibly aids in the carburization process by activating hydrogen and catalysing the support's activation to produce more available reactive carbon. Nevertheless, the MS profile of Cu/H, as shown in Fig. S5,† did not show the evolution of m/z = 15 which could indicate that the carburization is enhanced by a synergy between Cu and Mo. Alternatively, m/z = 15 could emerge from the reactions involving $MoO_xC_yH_z$ species to give Mo^0 and CH_4.

Still, the estimated XPS concentration of molybdenum carbide, oxycarbide and metallic species in both Mo_xC/H and $CuMo_xC/H$ activated at 600 °C or at 700 °C is quite similar and differences are only observed in the XRD patterns. These results seem to indicate that the carburization of the largest particles is favourable on the bimetallic sample, $CuMo_xC/H$, upon increasing the temperature up to 700 °C.

Surprisingly, the XPS results of the samples synthesized at 700 °C display a larger concentration of MoO_3 than those treated at 600 °C. Considering the XRD patterns of the *in situ* carburized and spent catalysts and D_2-TPD results, it could be inferred that some hydride species are transformed into oxide upon increasing the temperature. This transformation can take place in the presence of the as-formed water and would be also in agreement with the conclusions from the MS profiles regarding the reactions at temperatures above 600 °C.

At this point, we can also propose that in the fresh carburized catalysts, small $\beta\text{-}Mo_2C$ nanoparticles coexist along with larger oxycarbide particles detected by XRD. This conclusion agrees with the preferential carburization of the smallest particles in close contact with the support that we recently described.[14]

The carbothermal method using H_2 has been used for some carbon supports. For example, it has been reported that the synthesis of molybdenum carbide under H_2 over carbon nanofibers led to the formation of the oxycarbide phase at

550 °C, followed by the transformation into the β-Mo_2C phase starting at 650 °C.[16] Other examples can be found in which the β-Mo_2C phase was formed at 700 °C over carbon nanotubes under H_2 (ref. 12) and over activated carbon, the β-Mo_2C phase was detected at 800 °C.[13] There are few reports in the literature in which Mo^0 is present when a carbon support and H_2 as a carburization atmosphere are used. Rodríguez *et al.*[13] observed the formation of an unstable intermediate, MoO_xH_y, which was then converted to Mo^0 upon heating at 400 °C with a heating ramp of 10 °C min^{-1}. Similarly, Xiao *et al.*[20] evidenced a small proportion of Mo^0 on N, S, and P co-doped carbon nanospheres synthesised at 700 °C under diluted H_2. In contrast, Ochoa *et al.*[16] did not observe the formation of Mo^0 when fishbone-like carbon nanofibers were impregnated with the molybdenum precursor and treated up to 750 °C under H_2 atmosphere, with different heating ramps between 1 and 10 °C min^{-1}. The different reactivities of carbon atoms from the support could explain the differences. However, to the best of our knowledge, the carbon nanofibers used should not have a significantly higher proportion of reactive carbon than the other supports that could mask the formation of Mo^0. In that case, the reason might be also related to other experimental parameters that would require further study, such as the gas hourly space velocity during carburization which may influence the contact time with hydrogen.

2.2 Reaction results

The conversion of CO_2 was evaluated at 20 bar and different temperatures using $CuMo_xC$ (5 wt% Cu and 10 wt% Mo), monometallic Cu (5 wt% Cu) and Mo_xC (10 wt% Mo) supported on a high surface area graphite. Under these conditions, it was observed that the Cu-monometallic catalyst was not active, but it activated at either 250 °C (Cu/H) or 600 °C (not shown) under hydrogen, yielding values which are similar to those of the blank test. The main product obtained with all the catalysts was methanol. The methanol yields, as shown in Fig. 5, increased upon increasing the temperature up to 190 °C and 210 °C for Mo_xC/H and $CuMo_xC$/H, respectively, and then decreased due to the formation of CO through the reverse water gas shift reaction (RWGS). On the other hand, the yields of products CH_4 and CO, as shown in Fig. S6,† increase in the whole temperature range.

These results indicated that monometallic copper supported on the graphitic support employed is not active on the hydrogenation of CO_2 unlike Cu with a well-known behaviour supported on ZnO or ZrO_2 where CO_2 is adsorbed and activated on the oxide.[1,21] This agrees with simulations on pure Cu that proved weak CO_2 interaction with copper surfaces leads to low activity for CO_2 hydrogenation.[22,23] The copper surfaces on monometallic Cu/H that could be identified by TEM, as shown in Fig. S2,† are characterized from the TEM images by fast-Fourier transformation (FFT) and the (111) and (200) crystal planes, which agree with their apparently low ability to activate CO_2 in contrast to the activity of copper defective surfaces such as (311) and they are ascribed to Lewis acidity.[24]

In addition, the TEM images of $CuMo_xC$/H in Fig. 2a and b and Fig. S2† show that mainly highly dispersed Mo_xC particles of less than 3 nm are generated. The identification of these particles as Mo_xC is based on the results obtained by XRD and XPS. Moreover, individual large copper particles and/or agglomerates of copper particles, *ca.* 50–100 nm as shown in Fig. 2c, can be found and barely any physical contact was observed between Cu and Mo. Also, the proportion of the molybdenum phases, *i.e.* carbide and oxycarbide, on both Mo_xC/H and $CuMo_xC$/H estimated by XPS, as shown in Table 1, is similar. Hence, a synergy between Cu and Mo_xC is suggested.

Therefore, additional experiments with different Cu loadings were performed at 150 °C, in order to compare under differential conditions, and are shown in Fig. 6. The average yields of CH_3OH, CH_4 and CO increased upon increasing the copper content, and the highest copper loading reached values of *ca.* 0.21 μmol CH_3OH g^{-1} s^{-1}. It thus seems plausible that the observed large Cu particles

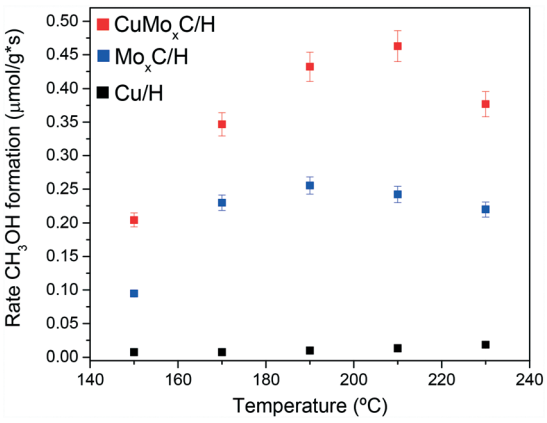

Fig. 5 Methanol formation rate per gram of catalyst at 20 bar, WHSV = 3600 h^{-1} and CO_2 : H_2 : He (1 : 3 : 6).

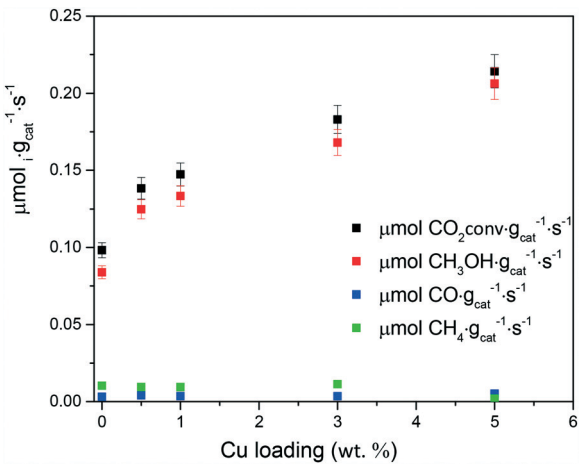

Fig. 6 CO_2 conversion rate and CH_3OH, CH_4 and CO formation rate at 20 bar, WHSV = 3600 h^{-1}, CO_2 : H_2 : He (1 : 3 : 6) and 150 °C.

coexist along with small Cu particles, even in the range of single metal atoms, scarcely detected by TEM/STEM or XRD as shown in Fig. 2d. The agglomeration of copper was indeed corroborated by the Cu/Mo atomic XPS ratio, as shown in Fig. S7,† which deviates from the theoretical value more significantly upon increasing the copper loading. Although the large Cu particles do not show any activity on the reaction as the results for the monometallic catalyst showed, the smallest Cu particles are located close to Mo_xC. In this case, the Cu–Mo_xC boundary would be the responsible for the synergy, increasing the conversion and selectivity to methanol.[25]

Then, we increased the carburization temperature for Mo_x-C/H and $CuMo_xC$/H to 700 °C aiming at reaching a higher proportion of carbide and better reaction yields. However, the results shown in Fig. 7 are actually the opposite of what is expected, and both the conversion rate of CO_2 and formation rate of methanol are lowered by 20–23% and 22–25%, respectively, compared to the values obtained with the catalysts prepared at 600 °C. Moreover, it can be observed that the selectivity to CO increases for the catalysts synthesized at 700 °C, which is more significant when using Mo_xC/H-700. A similar trend is observed for the selectivity to CH_4.

Stability tests for 24 hours at 230 °C were performed with Mo_xC/H and $CuMo_xC$/H carburized at 600 and 700 °C. The results, shown in Fig. 8, showed a stable profile for both catalysts prepared at 600 °C and at 700 °C.

Overall, the catalytic performance obtained with Mo_xC/H and $CuMo_xC$/H carburized at 600 °C and 700 °C is in line with their different proportions of Mo phases. The lower activity of Mo^0 compared to Mo_xC seems to be related to the formation of an HO_2C–Mo intermediate in which the scission of C–O is not energetically favourable.[26] Nevertheless, the catalytic results obtained suggest that at least some proportion of the as-formed Mo^0 particles are active and that

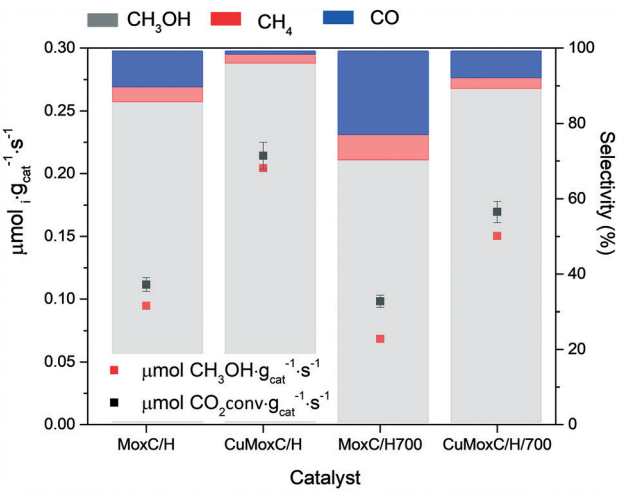

Fig. 7 CH_3OH formation rates and CO_2 conversion rates and selectivities at 20 bar. WHSV = 3600 h^{-1}, CO_2 : H_2 : He (1 : 3 : 6) and 150 °C.

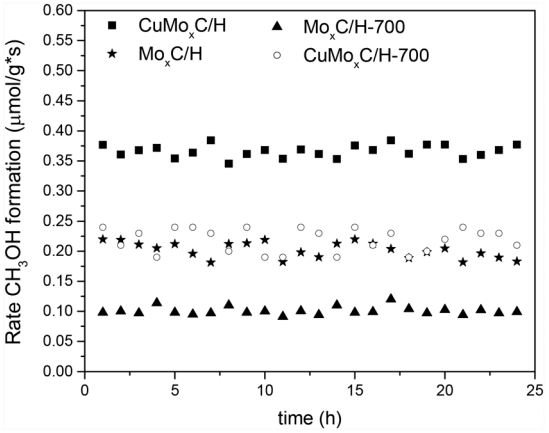

Fig. 8 CH_3OH formation rates at 20 bar. WHSV = 3600 h^{-1}, CO_2 : H_2 : He (1 : 3 : 6) and 230 °C.

they promote the selectivity to CO as the selectivity in Fig. 4 shows.

The XRD patterns of the spent catalysts after the reaction at 230 °C are shown in Fig. 1. The patterns of Mo_xC/H and $CuMo_xC$/H show diffractions at 2θ of 34.3°, 37.7° and 39.4° attributed to the β-Mo_2C phase and they are not observed on the fresh catalysts. On the other hand, the XRD pattern of the spent catalyst $CuMo_xC$/H-700 displayed a diffraction at 2θ of 39.9° not accompanied by that at 58°, which can then be attributed to MoO_3 likely resulting from Mo^0 oxidation.[27] With regards to the XRD pattern of spent Mo_xC/H-700, only a broad hump in the range of 35–39° is observed, also reflecting the instability of the Mo^0 species. The XPS analyses of the spent Mo_xC/H and $CuMo_xC$/H, as shown in Fig. S2,† only displayed one contribution of MoO_3, due to the unavoidable passivation layer.

The results indicate that once the hydride species are formed at 600 °C, the nanoparticles may follow two routes. Although the hydride particles under reaction conditions are transformed into β-Mo_2C, heating at 700 °C under H_2 leads to the formation of Mo^0.

As the XRD pattern of the spent catalyst showed, the Mo^0 particles are not chemically stable under the reaction conditions, and this likely explains why the large particles, which the XRD of the fresh catalyst showed, are not observed by microscopy where the samples are exposed to air. Moreover, the spent catalysts show diffractions at 2θ of 36.4° for $CuMo_xC$/H and 34.8° and 38.8° for $CuMo_xC$/H-700 which correspond to copper oxide.[28]

Also, since the catalysts' methanol yield was stable in the evaluated period, it is reasonable that the active phases are also stable and that the observed changes after the reaction correspond mostly to inactive species.

The synthesis of methanol using CO_2 hydrogenation may proceed by activation of CO_2 and conversion to CO *via* reverse water gas shift or formate/formaldehyde transformation into methanol. In general, molybdenum carbide suffers from deactivation when molecules with oxygen atoms are in the reaction atmosphere.[29] For example, during CO_2

hydrogenation over bulk catalysts, oxycarbides were identified as the most abundant species.[30] Under reaction, both phases, *i.e.* carbide and oxycarbide, coexist and are involved in a redox cycle where CO_2 reacts with Mo_2C through C–C interaction, producing oxycarbide and CO, which could eventually be reduced by hydrogen to obtain Mo_2C again. Based on the results obtained in the present work, we can add that the hydride can aid in the regeneration/formation of the carbide during the reaction.

Concerning the effect of copper, some previous literature regarding the catalytic performance of copper supported on ZnO or ZrO_2 in CO_2 hydrogenation suggested that the activation of hydrogen is boosted by copper; then, activated hydrogen is spilled over and reacts with the activated CO_2 adsorbed on molybdenum carbide.[31] Despite the D_2-TPD experiments as shown in Fig. S4† indicating that copper does not adsorb hydrogen at room temperature, we cannot rule out this phenomenon under reaction conditions. Nevertheless, the positive effect of Cu is confirmed since higher yields are obtained over $CuMo_xC/H$ and $CuMo_xC/H$-700 compared to Mo_xC/H.

The methanol production activities obtained in the present work with $CuMo_xC/H$ (see Fig. 5) are higher than the value reported for Cu supported on carbon nanofiber/ZrO_2, for which 0.2 μmol g^{-1} s^{-1} at 180 °C and 30 bar was reported,[31] and to that obtained with codoped nanospheres at 220 °C and 20 bar, which reached 0.24 μmol g^{-1} s^{-1}. The results obtained with other systems of the type Cu/ZnO or Cu/ZrO_2 offered 0.08–0.09 μmol g^{-1} s^{-1} activities to methanol at 250 °C and 20 bar.[32]

The obtained results proved that the carburization of molybdenum supported on high surface area graphite with H_2 not only produces active and selective molybdenum phases but also they are stable in the presence of oxygen species. This is relevant since one of the main problems of molybdenum and other transition metal carbides is their transformation into oxycarbides and oxides upon exposure to oxygen-containing molecules. Hence, the carbothermal conditions can be tuned to optimize the stability and regeneration of the catalyst. The results also highlight the difficulties in assessing the active phase by XRD as the most active phases are mainly small nanoparticles.

3. Experimental

3.1 Catalyst synthesis

The support employed was commercial high surface area graphite (HSAG400 from Timcal Graphite), labelled H (S_{BET} = 399 m^2 g^{-1}). Metal carbides were prepared by wet co-impregnation on this support with the corresponding metal precursors. An aqueous solution of the Mo precursor, $(NH_4)_6Mo_7O_{24}$ (99% from Aldrich), and Cu precursor, $Cu(NO_3)_2{\cdot}3H_2O$ (99% from Aldrich), was used to impregnate the support with an adequate amount to obtain the desired metal loading, left for maturation for 6 h, and dried overnight at 100 °C. The carburization was carried out for 2 h under pure H_2 at 600 or 700 °C (5 °C min^{-1}). The resulting catalysts were labelled according to the metal composition. The Mo loading was 10 wt% in all cases, while the Cu loading was 5 wt% in both the bimetallic and the monometallic samples, except in the catalysts where it is explicitly indicated to be 0.5, 1 and 3 wt%. Monometallic Cu supported on HSAG400 was also prepared by wet impregnation using the same metal precursor and activated at 250 °C (Cu/H) and 600 °C (Cu/H600) under H_2 for 2 h.

In this way, eight samples were prepared on HSAG400 and labelled: Cu/H; Cu/H600; Mo_xC/H; Mo_xC/H-700; $0.5CuMo_xC/H$ $1Cu/Mo_xC/H$; $3Cu/Mo_xC/H$; $CuMo_xC/H$; $CuMo_xC/H$-700.

3.2 Characterization

Textural properties of the samples were obtained from the N_2 adsorption isotherms at −196 °C, using a 3Flex instrument from Micromeritics. Around 100 mg of sample was previously degassed for 4 h at 120 °C under vacuum, using a SmartVacPrep instrument from Micromeritics. The surface area was calculated from the adsorption branch in the range of $0.02 \leq p/p_0 \leq 0.25$, using the Brunauer–Emmett–Teller (BET) model.

X-ray diffraction (XRD) patterns of the catalysts were acquired *in situ* by passing the corresponding atmosphere, H_2, using a reaction chamber (Anton Paar XRK900). The 2θ range was between 4° and 90°, with a step of 0.04° s^{-1}, using a Polycristal X'Pert Pro PANalytical diffractometer with Ni-filtered Cu Kα radiation (λ = 1.54 Å) operating at 45 kV and 40 mA. For the XRD patterns of the spent catalysts, the samples were passivated after the reaction by passing diluted O_2 for 2 hours at room temperature.

Photoelectron spectra (XPS) were recorded using an Escalab 200R spectrometer equipped with a hemispherical analyser and using non-monochromatic Mg Kα X-ray radiation ($h\nu$ = 1253.6 eV). The samples were treated under the same conditions as those used in the carburization and transferred to an octane solution to avoid oxidation, and transferred to an outgassing chamber. Prior to the experiments, the samples were outgassed *in situ* for 24 h to achieve a dynamic vacuum below 10^{-10} mbar. The binding energy (BE) was measured by reference to the C 1s peak at 284.6 eV, with an equipment error of less than 0.01 eV in the energy determination. The surface atomic ratios were estimated from the integrated intensities of Mo 3d, Cu 2p, C 1s and O 1s lines after background subtraction and correction by the atomic sensitivity factors. The spectra were fitted to a combination of Gaussian–Lorentzian lines of variable proportions.

TG-mass experiments were conducted with TA Instruments SDT Q600 TA equipment from 30 °C to 700 °C at 5 °C min^{-1} in H_2 flow (100 cm^3 min^{-1}, STP). The output gases from TGA were monitored by mass spectrometry using a ThermoStar GSD 301 T3 instrument (with a filament at 150 °C, SEM and emission detector at 950 mV). The m/z masses analysed were: 2, 18, 17,16, 15, 28 and 44.

For the D_2-TPD measurements, before each experiment, the catalyst sample (100 mg) was pretreated in a quartz reactor under hydrogen (H_2) flow for 2 hours at 600 °C, passed to a quartz bulb, outgassed under high vacuum and treated again under H_2 or a deuterium atmosphere at 500 °C for 1 hour. At ambient temperature, a deuterium pulse (30 Torr) was applied to the samples until equilibrium was reached and outgassed again under high vacuum. This step was omitted when the sample was treated with deuterium at 500 °C. Once stabilized, the temperature was raised to 500 °C at 10 °C min^{-1} monitoring the evolved gasses from the samples with a mass spectrometer (SRS-RGA200). Mass to charge ratios (m/e) obtained were 2, 3, 4, 16, 17, 18, 28, 32 and 44.

Information about the supported metal particles was acquired by TEM on a JEOL 2100F field emission gun electron microscope operated at 200 kV and equipped with an energy-dispersive X-ray detector. The samples were ground until powdered and a small amount was suspended in acetone using an ultrasonic bath. Some drops were added to the gold grid (Aname, Lacey carbon 200 mesh) and acetone was evaporated at room temperature before introducing to the microscope. Scanning transmission electron microscopy (STEM) was done using a spot size of 1 nm.

3.3 Reaction

The evaluation of the gas phase catalytic performance was carried out in a stainless steel fixed-bed flow reactor of 3/8″ internal diameter. The catalysts (0.5 g) were placed in the reactor and *in situ* carburized in pure H_2, by increasing the temperature up to 100 °C, keeping this temperature for 1 h and then raising it up to 600 °C or 700 °C, with a heating rate of 5 °C min^{-1}. The treatment at this temperature was carried out for 2 h. Finally, the catalysts were cooled under He to the reaction temperature, 150 °C. The reactor was pressurised at 20 bar using a reactant mixture composed of $CO_2:H_2:He$ = 1 : 3 : 6 vol, and the total flow during the reaction was 30 ml min^{-1}. The reactants and products were analyzed by gas chromatography (Varian CP 3400) with an FID and TCD, fitted with SupelQ Plot and 60/80 Carboxen-1000 columns, respectively.

The reaction conditions allowed the conversion in all the experiments to be maintained to assume a differential reactor. The carbon balance was over 95% in all cases, and blank tests resulted in a conversion below 0.5%. The conversion and product selectivity were obtained according to the following equations:

$$X_{CO_2} = \frac{\sum_i n_i \times mol_i}{\sum_i n_i \times mol_i + mol\,CO_2\text{-un}} \times 100 \quad (2)$$

$$S_i = \frac{n_i \times mol_i}{\sum_i n_i \times mol_i} \times 100 \quad (3)$$

where:

n_i: the number of carbon atoms of product i.
mol_i: the number of moles of product i.
$molCO_2$-un: mol of unreacted CO_2.

Conclusions

Overall, the characterisation showed differences depending on the carbothermal conditions. The XRD and XPS results of the Mo_xC/H catalyst displayed mainly MoO_xC_y/β-Mo_2C phases, indicating that incomplete carburization took place under the studied conditions. Also, D_2-TPD profiles showed that hydride species are formed. Increasing the carburization temperature up to 700 °C did not result in a larger extent of carburization and, in contrast, Mo^0 was obtained as the main phase. For the analogous samples containing Cu, similar results were obtained, but for the sample treated at 700 °C, the proportion of Mo^0 identified by XRD was lower compared to MoO_xC_y/β-Mo_2C, which is proposed to be a consequence of the enhanced H_2 activation by copper, favouring the production of CH_4 that would be the carburization source.

In addition, the incorporation of copper improves the catalytic performance, and this seems to happen even in the absence of nearby physical contact between Cu and Mo_xC. This can be explained by the presence of copper particles with few atoms and scarcely identified by microscopy, but the possibility of hydrogen activation on copper and spill over phenomena to β-Mo_2C cannot be ruled out.

Overall, the resulting catalysts are quite stable under reaction conditions although water is formed during the reaction, which is known to oxidize molybdenum carbide. However, the reaction may proceed through a path that implies a redox mechanism in which the molybdenum carbide is oxidized to an oxycarbide phase and further reduced again into the carbide by the hydrogen of the reactant feed. In this proposed mechanism, the exact role of the detected bulk hydride species needs further investigation.

Conflicts of interest

There are no conflicts to declare.

Acknowledgements

A. B. Dongil acknowledges financial support from the Fundación General CSIC (Programa ComFuturo and iLink project No 20211 from CSIC (Spain)). Financial support from the Spanish Agencia Estatal de Investigación (AEI) and EU (FEDER) (projects MAT2016-80285-P, CTQ2017-89443-C3-1-R and CTQ2017-89443-C3-3-R) is also acknowledged.

Notes and references

1 I. U. Din, M. S. Shaharun, M. A. Alotaibi, A. I. Alharthi and A. Naeem, *J. CO_2 Util.*, 2019, **34**, 20–33.
2 C. Li, X. Yuan and K. Fujimoto, *Appl. Catal., A*, 2014, **469**, 306–311.

3 D. W. Flaherty, S. P. Berglund and C. B. Mullins, *J. Catal.*, 2010, **269**, 33–43.
4 Y. Chen, S. Choi and L. T. Thompson, *J. Catal.*, 2016, **343**, 147–156.
5 W. Xu, P. J. Ramírez, D. Stacchiola, J. L. Brito and J. A. Rodriguez, *Catal. Lett.*, 2015, **145**, 1365–1373.
6 S. Posada-Pérez, P. J. Ramírez, J. Evans, F. Viñes, P. Liu, F. Illas and J. A. Rodríguez, *J. Am. Chem. Soc.*, 2016, **138**, 8269–8278.
7 J. Cao, J. Wang, Y. Ma, X. Li, P. Xiaokaiti, X. Hao, A. Abudula and G. Guan, *J. Alloys Compd.*, 2018, **735**, 1463–1471.
8 T. Huang, W. Huang, J. Huang and P. Ji, *Fuel Process. Technol.*, 2011, **2**, 1868–1875.
9 Z. Yao, J. Jiang, Y. Zhao, F. Luan, J. Zhu, Y. Shi, H. Gao and H. Wang, *RSC Adv.*, 2016, **6**, 19944–19951.
10 Z. Yao, F. Luan, Y. Sun, B. Jiang, J. Song and H. Wang, *Catal. Sci. Technol.*, 2016, **6**, 7996–8004.
11 P. Liang, H. Gao, Z. Yao, R. Jia, Y. Shi, Y. Sun, Q. Fan and H. Wang, *Catal. Sci. Technol.*, 2017, **7**, 3312–3324.
12 L. Souza Macedo, R. R. Oliveira, T. van Haasterecht, V. Teixeira da Silva and H. Bitter, *Appl. Catal., A*, 2019, **241**, 81–88.
13 W. Xu, P. J. Ramirez, D. Stacchiola and J. A. Rodríguez, *Catal. Lett.*, 2014, **144**, 1418–1424.
14 D. H. Carrales-Alvarado, A. B. Dongil, J. M. Fernández-Morales, M. Fernández-García, A. Guerrero-Ruiz and I. Rodríguez-Ramos, *Catal. Sci. Technol.*, 2020, **10**, 6790–6799.
15 J. Ding, X. Yan, B. K. Tay and Q. Xue, *J. Phys. Chem. Solids*, 2011, **72**, 1519–1523.
16 E. Ochoa, D. Torres, R. Moreira, J. L. Pinilla and I. Suelves, *Appl. Catal., A*, 2018, **239**, 463–474.
17 Y. Qin, L. He, J. Duan, P. Chen, H. Lou, X. Zheng and H. Hong, *ChemCatChem*, 2014, **6**, 2698–2705.
18 A. Tougerti, E. Berrier, A. S. Mamede, C. La Fontaine, V. Briois, Y. Joly, E. Payen, J. F. Paul and S. Cristol, *Angew. Chem., Int. Ed.*, 2013, **52**, 6440–6444.
19 E. Blanco, A. B. Dongil, J. L. García-Fierro and N. Escalona, *Appl. Catal., A*, 2020, **599**, 117600–117609.
20 W. Geng, H. Han, F. Liu, X. Liu, L. Xiao and W. Wu, *J. CO_2 Util.*, 2017, **21**, 64–71.
21 P. B. Rasmussen, P. M. Holmblad, T. Askgaard, C. V. Ovesen, P. Stoltze, J. K. Nørskov and I. Chorkendorff, *Catal. Lett.*, 1994, **6**, 373–381.
22 J. Nakamura, J. A. Rodriguez and C. T. Campbell, *J. Phys.: Condens. Matter*, 1989, **1**, SB149–SB160.
23 Y. Yang, J. Evans, J. A. Rodriguez, M. G. White and P. Liu, *Phys. Chem. Chem. Phys.*, 2010, **12**, 9909–9917.
24 K. Jonglack, B. B. Sarma, E. Andrés, N. Pfänder, P. Concepción and G. Prieto, *ACS Catal.*, 2019, **9**, 10409–10417.
25 S. Posada-Pérez, P. J. Ramírez, R. A. Gutiérrez, D. J. Stacchiola, F. Viñes, P. Liu, F. Illas and J. A. Rodriguez, *Catal. Sci. Technol.*, 2016, **6**, 6766–6777.
26 H. Tominaga and M. Nagai, *Appl. Catal., A*, 2005, **282**, 5–13.
27 M. Rahmani and K. Kalantar-Zadeh, *et al.*, *Sens. Actuators, B*, 2011, **145**, 13–19.
28 A. Dutta and M. Oezaslan, *et al.*, *J. Catal.*, 2020, **389**, 592–603.
29 A. Kumar, S. Phadke and A. Bhan, *Catal. Sci. Technol.*, 2018, **8**, 2938–2953.
30 M. D. Porosoff, X. Yang, J. A. Boscoboinik and J. G. Chen, *Angew. Chem., Int. Ed.*, 2014, **53**, 6705–6709.
31 Y. Chen, S. Choi and L. T. Thompson, *ACS Catal.*, 2015, **5**, 1717–1725.
32 H. Ren, C.-H. Xu, H.-Y. Zhao, Y.-X. Wang, J. Liu and J.-Y. Liu, *J. Ind. Eng. Chem.*, 2015, **28**, 261–267.